Predictive Cruise Control Using High-Definition Map and Real Vehicle Implementation

Hongqing Chu ⬤, Lulu Guo ⬤, Bingzhao Gao ⬤, Hong Chen ⬤, *Senior Member, IEEE*, Ning Bian, and Jianguang Zhou

Abstract—The development of high-definition (HD) maps has enabled predictive cruise control (PCC) systems to access additional road and traffic information. This study provides a novel control scheme of PCC, which utilizes HD map information. To minimize fuel consumption, the problem of the PCC is formulated as a nonlinear model predictive control, and the derivation and implementation of the fast solver are discussed. Then, a novel shift-map is proposed to define the different working regions to allow the application of the proposed PCC system. The use of the real-time HD map is discussed, and the proposed control scheme is evaluated through simulation and experimental tests. The total fuel-savings rates obtained with the PCC system and factory-installed ACC system over a 370 km route were compared. An average fuel-savings rate of as high as 8.73% can be obtained by the proposed PCC system.

Index Terms—Predictive cruise control, high-definition map, nonlinear MPC, real vehicle implementation.

I. INTRODUCTION

A VARIETY of automated systems has been added to vehicles by manufacturers and researchers in the past few decades. The gradually increasing levels of automation in vehicle driving have convinced consumers of the promising future of driverless vehicles [1]. Nowadays, many advanced driver-assistance systems (ADAS), such as adaptive cruise control (ACC), predictive cruise control (PCC), and autonomous emergency braking (AEB), have further extended the automation of navigation [2]. A growing number of production vehicles have been equipped with cruise control system as a key component of longitudinal vehicle motion control.

To meet stringent emission standards, studies on cruise control system have begun to focus on minimizing fuel consumption by optimizing operating-point power sources, driving styles, and transmission shift schedules. For example, in [3], [4], a pulse and gliding strategy is proposed to optimize driving behaviour from the perspective of periodic operation. In [5], a quadratic cost function is selected to smooth the desired acceleration. An optimal shift schedule of the transmission [6] can be used to improve fuel economy.

Predictive energy-saving technology [7], which is based on model predictive control (MPC), has attracted a tremendous attention with the development of modern microprocessors and information fusion technology. Luigi del Re *et al.* [8] presented a linear MPC approach to minimize the overall fuel consumption. Their approach proposes the direct penalization of fuel consumption. To minimize car following error and fuel consumption, the car-following model is formulated as a multiobjective optimization problem in [9], [10]. The solution to an indirect adaptive MPC for ACC system based on vehicle-to-vehicle communication is presented in [11].

Given that MPC-based cruise control strategies are dependent on the future road and traffic information, some studies have been conducted with road and traffic information [12], [13]. M. Kamal *et al.* [14] asserted that fuel consumption is greatly influenced by slope, and simulation results revealed that using the information of road gradients noticeably reduces fuel consumption. Velocity trajectory has been optimized using a global positioning system (GPS) and slope data, and experiments have shown that over a 120 km route, fuel consumption can be decreased by 3.5% without extending the trip time [15]. In [16], a predictive control system based on a roadway profile improved fuel economy by 4.2% compared with a conventional cruise control. In [17], the influence of traffic signals was analyzed on the basis of dynamic programming (DP). Traffic signals are used to formulate state and terminal constraints in problem formulation [18], [19]. The use of the preceding traffic information allow vehicles to avoid unnecessary braking [20]. This behavior is beneficial to reducing fuel consumption. Nowadays, the development of high-definition (HD) maps enables vehicles to access additional road and traffic information. Nevertheless, the utilization of the HD map for autonomous driving remains challenging.

In fact, researchers in cooperative ACC (CACC) field have often focused on theoretical analysis instead of on real vehicle implementation [21]. In particular, the real vehicle implemen-

tation of ACC using MPC is lacking, and related studies remain in the laboratory stage. Because such optimization problems can only be solved numerically [22], the computational burden of MPC restricts its application in real vehicle. In [23], the multiobjective problem of ACC system is transformed into an online quadratic programming (QP) problem with linear constraints. In the linear MPC framework, a numerical solution of the desired acceleration is obtained by using Dantzig-Wolfe's algorithm [24]. To efficiently solve optimal control problems, a computational framework was developed on the basis of explicit MPC [25]. In addition, many other numerical algorithms, such as Pontryagin's minimum principle (PMP), shooting methods and collocation methods, are expected to overcome the challenges posed by the real-time application of PCC [26].

This study aims to develop a PCC based on HD map information. The contributions of this study are summarized as follows. First, the problem of the PCC is formulated as a nonlinear MPC, and a fast solver is proposed. Second, a novel shift-map is constructed to define different working regions from the perspective of application. Third, HD map information is integrated into the PCC system in the form of dynamic map. Fourth, the total fuel consumptions obtained with the proposed PCC system and factory-installed ACC system over a 370 km route are compared. The proposed PCC system can obtain an average fuel-savings rate of as high as 8.73%.

The rest of this paper is organized as follows. The system model and optimal problem formulation are presented in Section II. The derivation of the real-time implementable optimal solution through PMP is discussed in Section III. The implementation of PCC with HD map information is discussed in Section IV. The proposed PCC scheme is evaluated through simulation and real vehicle experiments, and some main results are represented in Section V and Section VI. Finally, the conclusions are given in Section VII.

II. SYSTEM MODEL AND PROBLEM FORMULATION

The system model and the formulation of the predictive optimization problem with HD map are introduced in this section. The vehicle under investigation is a compact sport utility vehicle (SUV). Its power comes from a 2.0 L internal combustion engine (ICE) of 200 Nm mated to a 6-speed automatic transmission (AT). Actuators in the PCC system comprise the engine management system (EMS) and electronic stability control (ESC), which receive the commands of the engine torque and the braking deceleration, respectively. The actuators enable the longitudinal control of vehicle motion. As shown in Fig. 1, the HD map provides near-term future information, which consists of speed limit, slope, curvature and positioning message.

A. Vehicle Model

1) Traction and Coasting: According to Newton's second law, when the vehicle is operated in traction or coasting mode, its longitudinal dynamics has the following form.

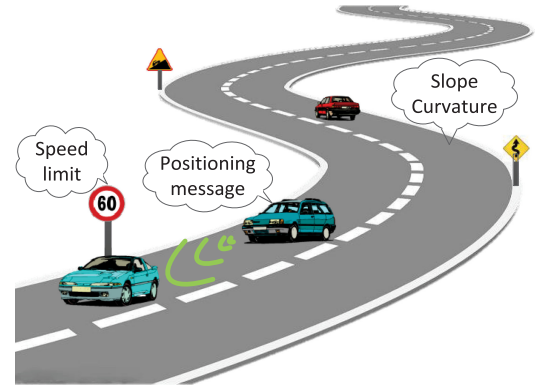$$\frac{v(k+1) - v(k)}{\Delta t} = \frac{F_t(k) - F_{\mathrm{arg}}(k)}{\delta m_v}, \tag{1}$$

Fig. 1. Predictive cruise control using HD map.

where $v(k)$ is the vehicle speed at step k, Δt is the discretization step, δ is the lumped rotational inertial coefficient, m_v is the vehicle mass, F_t is the traction force, F_{arg} is sum of the aerodynamic friction, the rolling friction, and the gravitational force.

The traction force is contributed by ICE, and the force that is equivalently applied to the tire can be described by

$$F_t(k) = \begin{cases} \frac{\eta_t I_0 I_g(k)}{r_w} T_e(k), & T_e(k) \geq 0 \\ \frac{I_0 I_g(k)}{\eta_t r_w} T_e(k), & T_e(k) < 0 \end{cases} \tag{2}$$

where η_t is the mechanical efficiency of the driveline, I_g is the transmission ratio, I_0 is the conversion ratio of final gears, r_w is the wheel effective radius, and T_e is the engine torque. Note that the traction force F_t that comes from ICE can be negative mainly because drag occurs when the engine stops injecting fuel. When $T_e(k) < 0$, ICE is power consumed. The mechanical efficiency η_t appears on the denominator, as given in Eq. (2).

The lumped longitudinal force is calculated as

$$F_{\mathrm{arg}}(k) = \frac{1}{2} C_D A \rho v^2(k) + m_v g(f \cos(\alpha(k)) + \sin(\alpha(k))), \tag{3}$$

where C_D is the aerodynamic drag coefficient, A is the frontal area, ρ is the density of ambient air, f is the rolling friction coefficient, g is the acceleration due to gravity, α is the slope angle. The road slope is a table with respect to the vehicle location.

2) Braking: When the vehicle is operated in braking mode, the longitudinal dynamics can be formulated as

$$\frac{v(k+1) - v(k)}{\Delta t} = \varphi_b(k) g, \tag{4}$$

where φ_b is the braking force coefficient. The braking force coefficient cannot increase infinitely. A limit is set on the basis of the maximum achievable braking deceleration, which depends on the situation between the tire and the road surface. The braking force coefficient cannot reach the limit during cruise control. If this situation is possible, in a well-developed ADAS, PCC is forced to shut down immediately, and AEB is activated to take over the control of the vehicle.

3) Fuel Consumption Rate: Fuel consumption of ICE is related to the engine speed, engine torque, temperature, etc. An accurate model of fuel consumption is critical for PCC. In this study, brake specific fuel consumption (BSFC) as a measure of

the fuel efficiency for ICE is used to model fuel consumption. It is typically obtained as an important engine map from engine manufacturers. The fuel consumption rate Q_f (its unit is [g/s]) is then expressed as a function of BSFC $Q_{BSFC}(T_e, \omega_e)$ (its unit is [g/(kWh)]),

$$Q_f(k) = Q_{BSFC}(T_e, \omega_e)P_e, \tag{5}$$

where P_e is the engine power. For the sake of simplicity, a two dimensional polynomial is fitted to represent the fuel consumption rate,

$$Q_f(k) = \sum_{i=0}^{2}\sum_{j=0}^{2} \iota_{i,j}T_e^i(k)\omega_e^j(k), \tag{6}$$

where $\iota_{i,j}$ is the coefficient to be fitted, and ω_e is the engine speed (its unit is [r/min]). Following the idea of approximating power losses in [27], the experimental data of the low-speed and low-torque region, which is an inefficient area, are disregarded to improve the accuracy of the model. This approach is reasonable because the optimal control will avoid working in this region. When the engine torque T_e is negative, the model of (6) is not applicable due to its possibility of fuel increase. In the negative torque situation, a small amount of fuel is considered to be consumed due to friction losses and heat dissipation. In this case, the engine torque T_e is set as 0 Nm. The relationship between the engine speed ω_e and the vehicle speed v has the following form.

$$\omega_e(k) = \frac{30}{\pi r_w}I_0 I_g(k)v(k) \tag{7}$$

B. Problem Formulation

This subsection will present the formulation of optimal problem for speed cruise mode and car-following mode. In these two modes, the actuator of PCC is ICE. The command of engine torque request is sent to EMS via controller area network (CAN).

1) Objective Function: The aim of the traditional ACC system is to maintain a steady speed, which is set by the driver, or automatically maintain a safe distance between the host vehicle and the preceding vehicle [28]. In actuality, the cruise control system is a tracking controller. In addition, as described in [29], the fuel consumption rate of ICE has a characteristic S-shaped nonlinearity. As a matter of fact, this characteristic enables the addition of a fuel-saving nature to the PCC. Based on the traditional ACC, we consider the fuel consumption rate of ICE to formulate the optimal tracking control problem. Therefore, the PCC is summarized as a nonlinear multiobjective optimization. Suppose the reference speed v_{ref} is given. The objective function to be minimized is formulated as

$$J = \sum_{k=0}^{N-1} F(v(k), T_e(k))\Delta t + \kappa(v(N) - v_{ref})^2 \tag{8}$$

where $F(v(k), T_e(k))$ is selected as

$$F(v(k), T_e(k)) = Q_f(k) + \kappa_1(v(k) - v_{ref})^2$$
$$+ \kappa_2(T_e(k+1) - T_e(k))^2, \tag{9}$$

N is the predictive horizon, and $\kappa, \kappa_1, \kappa_2$ are the weighting coefficients. Clearly,

- penalty item $Q_f(k)$ is added to minimize the fuel consumption, i.e., ensure that ICE always works in the high efficiency area;
- penalty item $(v(k) - v_{ref})^2$ forces the tracking error to converge to zero;
- penalty item $(T_e(k+1) - T_e(k))^2$ ensures the vehicle smoothly accelerates and improves vehicle comfort by reducing the fluctuation of the engine toque T_e;
- penalty item $(v(N) - v_{ref})^2$ is a terminal constraint that guarantees that the vehicle reaches the reference speed at step N.

After a careful consideration, penalty item $Q_f(k)$ and penalty item $(v(k) - v_{ref})^2$ are easily found to be contradictive. The perfect tracking of a speed reference often occurs at the expense of increasing fuel consumption. Therefore, the choice of the weighting coefficients is a tradeoff.

2) Capacity Constraints: First, the engine torque $T_e(k)$ has a capacity constraint from ICE, namely,

$$T_{e,\min}(\omega_e(k)) \leq T_e(k) \leq T_{e,\max}(\omega_e(k)). \tag{10}$$

The performance of longitudinal acceleration is limited not only by engine power but also by the traction limits of the drive wheels. On the assumption that the driving tire has no or negligible slip, the longitudinal acceleration is limited by the friction coefficient between the tire and the road. In the development of PCC, the vehicle under investigation can be reasonably assumed to work on a dry road. The constraint of the longitudinal acceleration is approximately expressed as

$$\sigma\varphi_{\min}g \leq \frac{v(k+1) - v(k)}{\Delta t} \leq \sigma\varphi_{\max}g, \tag{11}$$

where σ is the conservative coefficient. Typically, on a dry asphalt road, the value of $\varphi_{\max}$ is between $0.7 \sim 0.8$, and the value of $\varphi_{\min}$ is between $-0.9 \sim -0.8$.

Second, considering the speed limit information and applicability under low-speed conditions, a constraint of maximum and minimum speed is added,

$$v_{\min} \leq v(k) \leq v_{\max}. \tag{12}$$

Note that the maximum speed limit $v_{\max}$ can be obtained from road speed limits, road curvature information, and maximum vehicle design speed.

3) Safety Constraints: In the car-following scenario, a minimum safe distance should be considered to avoid collision. The dynamics of two vehicles in the car-following scenario is

$$\frac{s(k+1) - s(k)}{\Delta t} = v_p(k) - v(k), \tag{13}$$

where s is the inter-vehicle distance and is definitely $s > 0$, and v_p is the speed of the preceding vehicle. As for the minimum safe distance, an arbitrary car-following scenario is considered in [30], which points out human reaction time can be eliminated to improve performance. Here, a spacing policy with constant time headway is adopted,

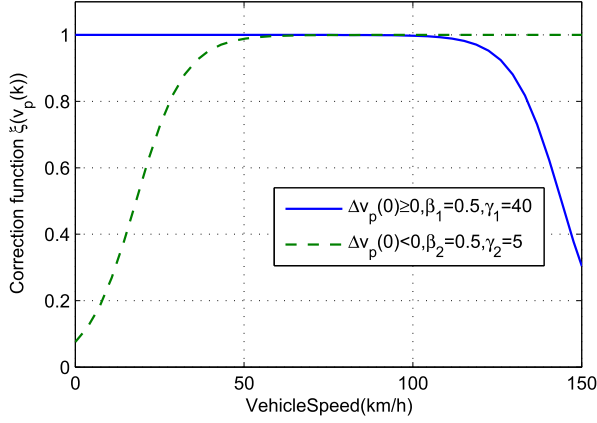$$s(k) \geq s_{\min,0} + \tau_{\min}v(k), \tag{14}$$

Fig. 2. Correction function in prediction model (15).

where $s_{\min,0}$ is the minimum inter-vehicle distance when the vehicle is at stand still, and $\tau_{\min}$ is the minimum time headway.

4) Future Speed of the Preceding Vehicle: The future speed of the preceding vehicle is related to traffic flow, driving style, etc [31]. To accurately estimate the future speed information of the preceding vehicle, a correction function can be added to simulate the actual driving behavior. In [20], assuming that the states of the preceding vehicle will hold until the states reach saturation, the acceleration of the preceding vehicle in the prediction horizon is estimated. It is quite suitable for the car-following conditions of PCC. In this paper, the following relationship is used,

$$\Delta v_p(k) = \Delta v_p(0)\xi(v_p(k))$$

$$\xi(v_p(k)) = \begin{cases} \frac{1}{1+e^{\beta_1(v_p(k)-\gamma_1)}} & \Delta v_p(0) \geq 0 \\ \frac{1}{1+e^{-\beta_2(v_p(k)-\gamma_2)}} & \Delta v_p(0) < 0 \end{cases}, \quad (15)$$

where $\Delta v_p(k) = v_p(k+1) - v_p(k)$ is the difference operator, $\xi(v_p(k))$ is the correction function, β_1 and β_2 are the sharpness coefficients, and γ_1 and γ_2 are the range coefficients. The correction function is shown in Fig. 2. When the preceding vehicle is in the acceleration scenario, i.e., $\Delta v_p(0) > 0$, the acceleration will decrease with the increasing of the vehicle speed $v_p(k)$. The acceleration approaches zero when the preceding vehicle reaches a maximum velocity (to ensure that the vehicle speed does not always increase). Similarly, when the preceding vehicle is in the deceleration scenario, i.e., $\Delta v_p(0) < 0$, the acceleration will decrease with the decreasing of the vehicle speed $v_p(k)$. The acceleration approaches zero when the preceding vehicle stops (to ensure that the preceding vehicle does not move backward).

5) Reference Speed: In the car-following scenario, the desired speed v_{des} is determined by using a desired time headway τ_{des}. At step N, the inter-vehicle distance $s(N)$ is expected to equal the desired distance, namely, $s(N) = v_{des}\tau_{des}$ (the constraints (14) hold).

For distance calculation, the assumption that the acceleration of the host vehicle is constant in the predictive horizon is reasonable, i.e.

$$s(N) = s(0) + \sum_{k=0}^{N-1} \left(v_p(k) - \frac{v_{des} + v(0)}{2}\right)\Delta t. \quad (16)$$

Then, the terminal constraint $(v(N) - v_{ref})^2$ is transformed into tracking a inter-vehicle distance.

The reference speed can be easily obtained for other scenarios. For instance, when there is no preceding vehicle, the reference speed is cruise speed set v_{set}. In summary, by combining the speed limit v_{lim}, the desired speed v_{des}, the cruise speed set v_{set}, and the allowable speed in curve conditions v_{cir}, the given reference speed can be written as

$$v_{ref} = \min\{0.9v_{lim}, v_{des}, v_{set}, v_{cir}\}. \quad (17)$$

6) Formulation Summary: To summarize, the optimization problem of the PCC can be formulated as follows,

$$\min_{T_e}:$$

$$J = \sum_{k=0}^{N-1} F(v(k), T_e(k))\Delta t + \kappa(v(N) - v_{ref})^2 \quad (18a)$$

subject to:

$$\frac{v(k+1) - v(k)}{\Delta t} = \frac{F_t(k) - F_{arg}(k)}{\delta m_v} \quad (18b)$$

$$\frac{s(k+1) - s(k)}{\Delta t} = v_p(k) - v(k) \quad (18c)$$

$$T_{e,\min}(\omega_e(k)) \leq T_e(k) \leq T_{e,\max}(\omega_e(k)) \quad (18d)$$

$$\sigma\varphi_{\min}g \leq \frac{v(k+1) - v(k)}{\Delta t} \leq \sigma\varphi_{\max}g \quad (18e)$$

$$v_{\min} \leq v(k) \leq v_{\max} \quad (18f)$$

$$s(k) \geq s_{\min,0} + \tau_{\min}v(k) \quad (18g)$$

Clearly, this problem is a nonlinear MPC with respect to the control sequences $T_e(0), T_e(1), \ldots, T_e(N-1)$. In accordance with MPC strategy, at each step, a feasible solution is obtained for the optimization problem (18), and the first element of the obtained control sequences is applied to the PCC system. At the following step, the procedure is repeated with new state measurements. In predictive horizon, the transmission ratio I_g is regarded as a constant. To obtain a fast solver for real time implementation, the constraints of (18c) and (18g) are addressed by a schedule solution, and detailed information will be given in Section IV and Section VI.

III. PREDICTIVE CRUISE CONTROL

The derivation of a fast solver for the optimization problem shown in (18) is discussed in this section. An indirect method based on PMP is used to find a real-time implementable optimal solution.

A. Pontryagin's Minimum Principle

As for the optimization problem (18), given that the inter-vehicle distance $s(k)$ does not appear in the objective function

(18a), the Hamiltonian in discrete time is defined to be

$$H(v(k), \lambda(k+1), T_e(k)) = F(v(k), T_e(k))$$
$$+ \lambda(k+1)\left(\frac{F_t(k) - F_{\arg}(k)}{\delta m_v}\right)\Delta t, \quad (19)$$

where $\lambda(k+1)$ is the costate variable. PMP states that the optimal control input T_e^* must satisfy:

$$H(v^*(k), \lambda^*(k+1), T_e^*(k)) \leq H(v^*(k), \lambda^*(k+1), T_e(k)),$$
$$k \in [0, 1, \ldots, N-1] \quad (20)$$

where $v^*(k) \in \Omega_1[0, 1, \ldots, N-1]$ is the optimal trajectory of the vehicle speed, and $\lambda^*(k+1) \in \Omega_2[0, 1, \ldots, N-1]$ is the optimal trajectory of the costate variable. In addition, the equations of the costate variable are given as

$$\lambda(k+1) = -\frac{\partial H(v(k), \lambda(k+1), T_e(k))}{\partial v(k)} + \lambda(k) \quad (21a)$$

$$\lambda(N) = 2\kappa(v(N) - v_{ref}) \quad (21b)$$

To provide some clarity, by substituting (2), (3), (6) and (7) into (19), expansions of the Hamiltonian (19) both in powers of $T_e(k)$ and in powers of $v(k)$ are reformulated by

$$H(v(k), \lambda(k+1), T_e(k)) = \varrho_1(k)T_e^2(k) + \varrho_2(k)T_e(k)$$
$$+ \varrho_3(k) = \varrho_4(k)v^2(k) + \varrho_5(k)v(k) + \varrho_6(k), \quad (22)$$

where

$$\varrho_1(k) = \sum_{j=0}^{2}\iota_{2,j}\omega_e^j(k) + \kappa_2,$$

$$\varrho_2(k) = \sum_{j=0}^{2}\iota_{1,j}\omega_e^j(k) + \lambda(k+1)\Delta t\frac{\eta_t I_0 I_g(k)}{\delta m_v r_w}$$
$$- 2\kappa_2 T_e(k+1),$$

$$\varrho_3(k) = \sum_{j=0}^{2}\iota_{0,j}\omega_e^j(k) + \kappa_1(v(k) - v_{ref})^2$$
$$+ \kappa_2 T_e^2(k+1) - \frac{\lambda(k+1)\Delta t}{\delta m_v}F_{\arg}(k),$$

$$\varrho_4(k) = \sum_{i=0}^{2}\iota_{i,2}T_e^i(k)\left(\frac{30 I_0 I_g(k)}{\pi r_w}\right)^2 + \kappa_1$$
$$- \frac{\lambda(k+1)}{2\delta m_v}\Delta t C_D A\rho,$$

$$\varrho_5(k) = \sum_{i=0}^{2}\iota_{i,1}T_e^i(k)\left(\frac{30 I_0 I_g(k)}{\pi r_w}\right) - 2\kappa_1 v_{ref},$$

$$\varrho_6(k) = \sum_{i=0}^{2}\iota_{i,0}T_e^i(k) + \kappa_1 v_{ref}^2 + \kappa_2(T_e(k+1) - T_e(k))^2$$
$$+ \frac{\lambda(k+1)}{\delta m_v}\Delta t(F_t(k) - m_v g(f\cos(\alpha(k))$$
$$+ \sin(\alpha(k)))).$$

By substituting (22) into (21a), the update equation of the costate variable $\lambda(k+1)$ is derived as

$$\lambda(k+1) = -2\varrho_4(k)v(k) - \varrho_5(k) + \lambda(k). \quad (23)$$

Given that $\varrho_4(k)$ is an explicit function of $\lambda(k+1)$, substituting $\varrho_4(k)$ into (23) leads to

$$\lambda(k+1) = \lambda(k) - \varrho_5(k)$$
$$- 2\left(\sum_{i=0}^{2}\iota_{i,2}T_e^i(k)\left(\frac{30 I_0 I_g(k)}{\pi r_w}\right)^2 + \kappa_1\right)v(k), \quad (24)$$

where $\frac{\delta m_v}{\delta m_v - \Delta t C_D A\rho v(k)} \approx 1$ is used.

From expansions (22), we can see that, to obtain the extremum of the Hamiltonian, the constraint of the optimal control input $T_e(k)$ is first needed. In accordance with the restrictions of (18d), (18b) and (18e), the explicit constraints of the optimal control input $T_e(k)$ are obtained as,

$$\overline{T_e(k)} = \min\left\{T_{e,\max}(\omega_e(k)), \frac{r_w(\delta\sigma\varphi_{\max}m_v g + F_{\arg}(k))}{\eta_t I_0 I_g(k)}\right\}$$

$$\underline{T_e(k)} = \max\left\{T_{e,\min}(\omega_e(k)), \frac{r_w(\delta\sigma\varphi_{\min}m_v g + F_{\arg}(k))}{\eta_t I_0 I_g(k)}\right\} \quad (25)$$

According to PMP, the explicit optimal control input is obtained to minimize the Hamiltonian (22),

$$T_e^{opt}|_{\varrho_1(k)>0} = \begin{cases} -\frac{\varrho_2(k)}{2\varrho_1(k)} & \underline{T_e(k)} \leq -\frac{\varrho_2(k)}{2\varrho_1(k)} \leq \overline{T_e(k)} \\ \overline{T_e(k)} & -\frac{\varrho_2(k)}{2\varrho_1(k)} > \overline{T_e(k)} \\ \underline{T_e(k)} & -\frac{\varrho_2(k)}{2\varrho_1(k)} < \underline{T_e(k)} \end{cases}$$

$$T_e^{opt}|_{\varrho_1(k)<0} = \begin{cases} \overline{T_e(k)} & \underline{T_e(k)} \leq -\frac{\varrho_2(k)}{2\varrho_1(k)} \leq \overline{T_e(k)}, \\ & \text{and } H(\underline{T_e(k)}) > H(\overline{T_e(k)}) \\ \underline{T_e(k)} & \underline{T_e(k)} \leq -\frac{\varrho_2(k)}{2\varrho_1(k)} \leq \overline{T_e(k)}, \\ & \text{and } H(\underline{T_e(k)}) \leq H(\overline{T_e(k)}) \\ \underline{T_e(k)} & -\frac{\varrho_2(k)}{2\varrho_1(k)} > \overline{T_e(k)} \\ \overline{T_e(k)} & -\frac{\varrho_2(k)}{2\varrho_1(k)} < \underline{T_e(k)} \end{cases}$$

$$T_e^{opt}|_{\varrho_1(k)=0} = \begin{cases} \overline{T_e(k)} & \varrho_2(k) < 0 \\ 0 & \varrho_2(k) = 0 \\ \underline{T_e(k)} & \varrho_2(k) \geq 0 \end{cases} \quad (26)$$

B. Implementation of the Fast Solver

Benefiting from the explicit optimal control input (26) and the update equation of the costate variable (24), the terminal value $\lambda(N)$ can be represented as a function with the argument of $\lambda(0)$, defined as $\lambda(N) = F(\lambda(0))$. If the initial value of the costate variable $\lambda(0)$ can be found such that the terminal condition (21b) is satisfied, i.e., $F(\lambda(0)) = 2\kappa(v(N) - v_{ref})$, the numerical solution of the original optimization problem (18), the control sequences $T_e(0), T_e(1), \ldots, T_e(N-1)$, can be obtained.

Algorithm 1: Fast Algorithm for Solving PCC Problem.

Initialization: set vehicle parameters and controller
           parameters;
Update: measure the states of host vehicle and the
           preceding vehicle;
Map: obtain the road information of the prediction
           horizon from the HD map;
Prediction: estimate the future speed information of the
           preceding vehicle on the basis of Eq.(15);
Iteration initialization: set $\lambda(0)$ and $r = 0$;
repeat
    update: adjust $\lambda(0)$ using bisection method;
repeat
    set k = 0;
    predict $T_e(k)$ and $\lambda(k+1)$ on the basis of Eq. (25)
    and Eq. (26);
    until $k = N - 1$
until $\beth(\lambda^{(r)}(0)) \leq \varepsilon$
Return $T_e(0)$;

Fig. 3.   Shift-map for implementation.

As described above, the original optimization problem (18) is formulated as a problem of finding roots of nonlinear equation. Given that the nonlinear equation of PCC problem is a continuous function and it is difficult to obtain the function's derivative, the bisection method is used to find a feasible root in this study. The iteration of the bisection method stops when the following relationship is met, i.e.,

$$\beth(\lambda^{(r)}(0)) := F(\lambda^{(r)}(0)) - 2\kappa(v(N) - v_{ref}) \leq \varepsilon. \quad (27)$$

where r is the number of iterations, and ε is the tolerance. The method is guaranteed to converge to a root of $\beth(\lambda^{(r)}(0))$ if $\beth(\lambda^{(r)}(0))$ is a continuous function defined on the interval $[\lambda_L, \lambda_U]$ and $\beth(\lambda_L)$ and $\beth(\lambda_U)$ have opposite signs. The convergence analysis has been given in Appendix.

The overall fast solver of the optimization problem of the PCC can be summarized as in Algorithm 1.

IV. IMPLEMENTATION OF PCC WITH HD MAP

The optimal control input (26) can not apply to all working conditions. In addition, the actuators of PCC are EMS and ESC, and they do not work simultaneously. Therefore, a novel shift-map is proposed to provide a schedule for different working conditions. The information integration of HD map will then be described in this section.

A. Shift-Map

From the perspective of application, the operating mode of a vehicle with PCC is divided into four modes, namely, speed cruise mode, car-following mode, coasting mode, braking mode. These modes are illustrated in Fig. 3. The hold region is introduced to avoid frequent mode switching.

The speed cruise mode and the car-following mode are based on the optimization problem, which is given in (18). As shown in Fig. 3, when there is no preceding vehicle or the actual
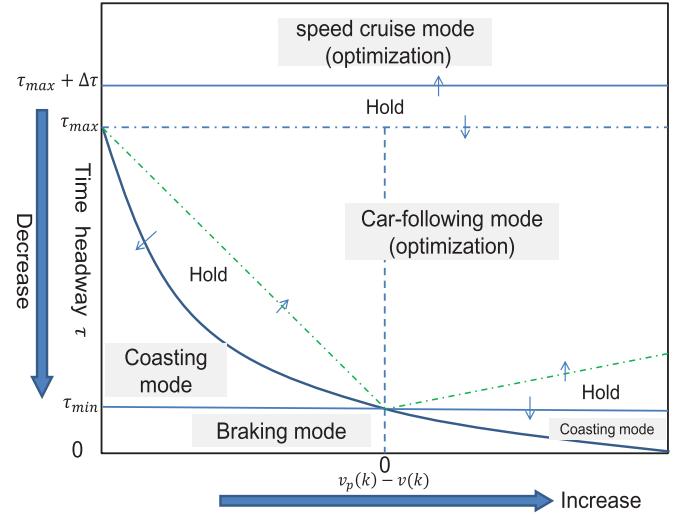
time headway exceeds the maximum time headway in the car-following scenario, the system enters the speed cruise mode. The difference between speed cruise mode and car-following mode lies in the choice of the reference speed, which is discussed in Eq. (17).

In the coasting mode, the control inputs, namely, the commands of the engine torque and the braking deceleration, are set to zero.

$$T_e = 0$$
$$\varphi_b = 0. \quad (28)$$

Note that when the engine torque request is zero and the engine speed exceeds a given value, such as 2000 rpm, the ignition is turned off by engine control unit (ECU) for the investigated vehicle. It is helpful for the fuel saving. By assuming that the vehicle is operated in an idealized condition, the time headway can be expressed as a quadratic function of $v_p(k) - v(k)$, as described in [3]. Thus, a quadratic curve is selected as the shifting line between car-following mode and coasting mode.

In the braking mode, a prescribed lookup table is used to determine the braking deceleration

$$T_e = 0$$
$$\varphi_b = fmap(\tau, v), \quad (29)$$

where $fmap(\tau, v)$ is a prescribed lookup table with respect to time headway and host vehicle speed. When the vehicle speed is greater than the maximum speed limit v_{lim}, i.e., the constraint of (18f) is violated, the system enters the braking mode. As shown in Fig. 3, when the actual time headway is less than the minimum time headway, i.e., the constraint of (18g) is violated, the system enters the braking mode. In addition, braking is inevitable in the cut-in scenario under the conventional constant-headway control due to the sudden decrease of the time headway. However, the speed of cut-in vehicle is often faster than that of host vehicle. The actual time headway increases with time phase, as described in (18c). In this case, coasting is better than

braking, because it can save energy. The proposed shift-map allows vehicle to coast in this driving scenario, as shown in lower right area of Fig. 3.

A low-speed cruise mode or stop-and-go mode is usually introduced to deal with low-speed conditions. Under these conditions, the fuel consumption model is inaccurate, meanwhile, the precise control of the engine torque is difficult. These make fuel-saving potential limited. In addition, safety and comfort are more important than fuel economy [32]. Therefore, the proposed PCC is not applicable. In the implementation, a lookup table-based method is used for the low-speed cruise mode. When vehicle speed is less than a speed threshold, such as 20 km/h, PCC is deactivated, and the low-speed cruise mode is activated. Similarly, when vehicle speed is larger than another speed threshold, such as 30 km/h, the low-speed cruise mode is deactivated and PCC is activated. The hold region from 20 km/h to 30 km/h is introduced to avoid frequent mode switching. The selection of the speed threshold is based on the average speed of congested expressway [33].

B. Use of HD Map

The application of HD map remains in the laboratory stage. Compared with the usual standard definition (SD) map, HD map allows vehicle to locate itself more precisely and to build a more detailed model of the surrounding environment. The HD refers to an increase in vehicle positioning precision and map data accuracy over a previously used standard. The accuracy requirement of PCC map is less than that of autonomous driving map. In the PCC application, the positioning devices are differential GPS and inertial navigation system (INS). When GPS signals are lost, INS is used to estimate position information. The HD map for PCC application offers a positioning accuracy of ± 3 m, a slope accuracy of ± 2 m/100 m (ratio of elevation error to horizontal distance), and a curvature accuracy of $\pm 10\%$.

Large volumes of data are being collected in the HD map. The collected data of the HD map are divided into numerous small sections and stored in an in-car user interface media system. The automotive navigation software, which is on the in-car user interface media system, provides a planned path according to the needs of the driver. There are lots of the small sections along the planned path. Storing the overall data of the planned path is impossible because of the storage limitation of PCC hardware. For this reason, the hardware system for PCC implementation only stores a piece of map data by using the dynamic map. The piece of map data should be long enough to provide the near-term future information for PCC. The span of the dynamic map is set to 300 m in real-time implementation because the traveling distance of the host vehicle can not be more than 300 m during the prediction horizon. The dynamic map is first-in first-out. As the vehicle moves forward, the old data of the dynamic map are replaced by the new data, and the PCC is then implemented with the new near-term future information.

The data transmission mechanism is shown in Fig. 4. In accordance with the current location of the vehicle, the future data of the HD map are transmitted to the PCC hardware from the in-car user interface media system via CAN. The data transmission
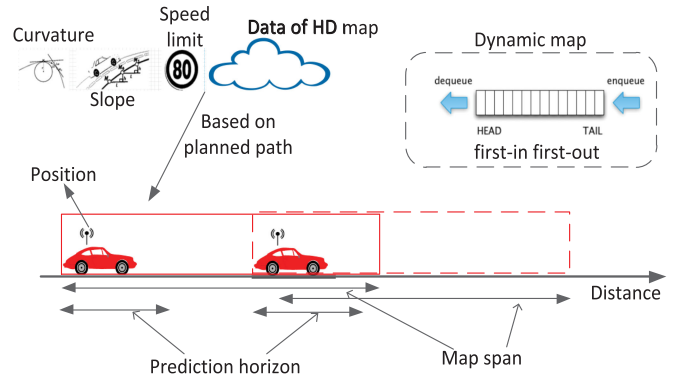

Fig. 4. Transmission mechanism of HD map information.

mechanism is triggered. Every time the data undergo change, CAN will transmit the location-depended data to the PCC hardware. The location-depended data are then stored in the dynamic map. The near-term future information of road condition is thus available to the proposed PCC. Furthermore, the location of the vehicle will sometimes be lost given the loss of GPS signals. In this case, the flag of the loss of GPS will be transmitted to the vehicle. The information of HD map is invalid, and PCC does not use the data.

In the application of PCC, slope, speed limit and curvature are used. The following will give detailed information.

1) Slope: The accurate slope in the predictive horizon is crucial to guarantee the accuracy of the predictive model. As described in Eq. (3), the slope resistance that is caused by the slope of 1 degree is equivalent to 1.5 times the rolling resistance of the vehicle. In real-time implementation, the slope is location-depended and stored in the dynamic map. As mentioned above, the span of the dynamic map is longer than the span required to implement PCC. In the predictive horizon, the future slope information is obtained by looking up the dynamic map according to the future location of the vehicle. Thus, the future slope information is introduced into the optimization problem of the PCC by Eq. (18g) and Eq. (3). To reduce the computation time, an inherited method can be used to search the dynamic table. Given that vehicle location in predictive horizon is consistently increasing, the table can be searched from the last index.

2) Speed Limit and Curvature: Speed limit information is used as a speed constraint, as described in Eq. (18). Curvature is used to obtain a reference speed under curve conditions. The vehicle under curve conditions is undergoing acceleration by a centripetal force. According to Newton's laws of motion, the speed is limited by the permissible lateral acceleration $a_{lateral,\max}$ [34], i.e.,

$$v_{cir} = \sigma_v \sqrt{R_{\min} a_{lateral,\max}}, \qquad (30)$$

where σ_v is the conservative coefficient, and $R_{\min}$ is the minimum curvature radius of the curved road.

Considering positioning error and overall length of vehicle, the information of speed limit and curvature is pushed forward at a certain offset, such as 10 m. For instance, when the host vehicle approaches a curve, the reference speed v_{cir} is a minimum speed
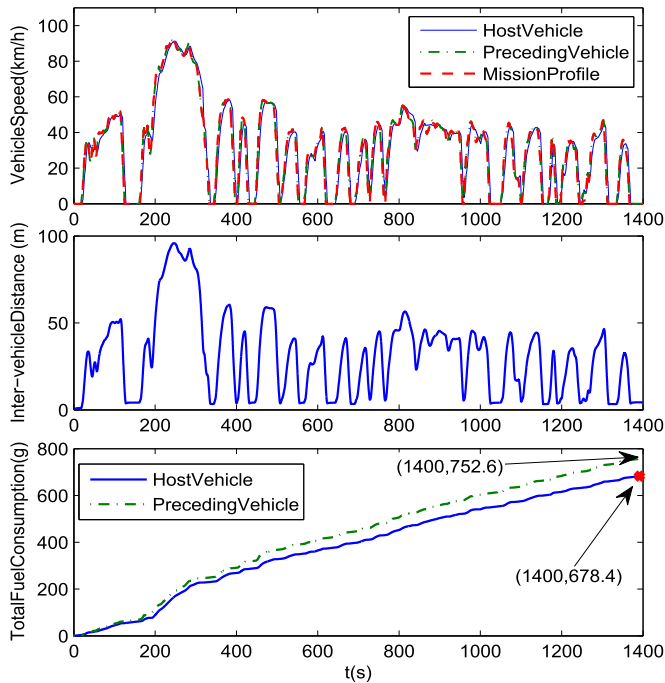
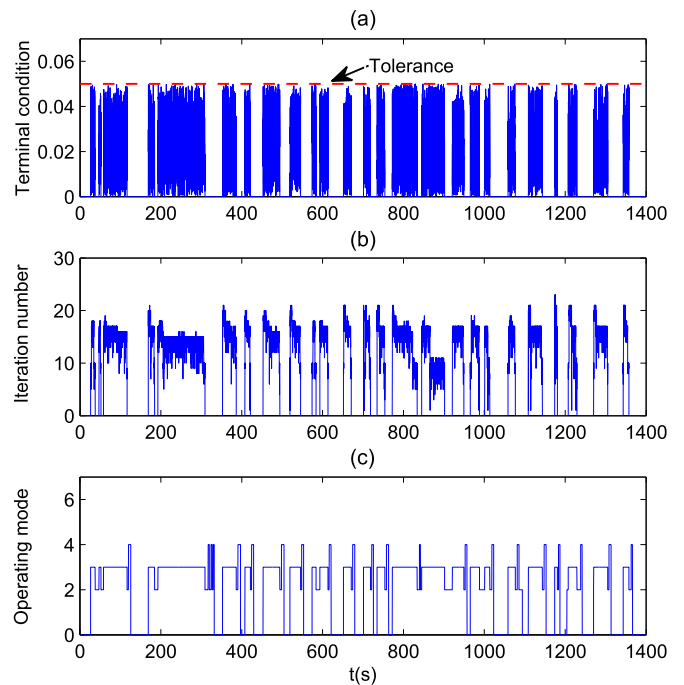Fig. 5.   Simulation results: the driving cycle of UDDS.

Fig. 6.   Iteration results. (a) Terminal condition at the end of iteration. (b) Iteration number. (c) Operating mode (1: speed cruise mode 2: coasting mode 3: car-following mode 4: braking mode 0: low-speed cruise mode).

in this offset horizon from the current vehicle position to the offset position.

V. SIMULATION RESULTS

To validate the proposed PCC scheme and observe energy efficiency, the model of two SUVs with 6-speed AT is constructed using the commercial software AMEsim, and the proposed PCC is built in Matlab/Simulink. The AT system allows ICE to provide a range of speed and torque outputs by automatic gear-shifting as the vehicle moves. In the simulation, a well-developed gear shift-map is used to determine an appropriate gear ratio. The gear shift-map is based on the driving velocity and the throttle valve position [35], [36].

The parameters of the investigated vehicle are same as those of the preceding vehicle in the simulation. For the host vehicle, the current speed of the preceding vehicle is regarded as known, whereas the future speed is unknown. The future speed in predictive horizon is obtained via the model of (15). The two SUVs are assumed to be driving on a flat road. The initial inter-vehicle distance is 0 m, and the cruise speed set is 30 m/s.

A. Performance and Convergency

The preceding vehicle is controlled by a driver model to track the mission profile of urban dynamometer driving schedule (UDDS). The host vehicle is controlled by the proposed PCC to simulate a car-following scenario. The simulation results are presented in Fig. 5. Consistent with actual driving experience, inter-vehicle distance varies with the vehicle speed. Compared with that of the preceding vehicle, the fuel economy of the vehicle with the proposed PCC has increased by 10.9%. In addition, new European driving cycle (NEDC) is also used as

a mission profile for the preceding vehicle. Its benefit in fuel consumption is up to 6%.

To further observe the convergence of the proposed solver, the iteration results are given in Fig. 6 for the driving cycle of UDDS. It can be seen that the proposed solver can guarantee convergence to the optimal solution (the integrated terminal condition is less than the specified tolerance, as described in Eq. (27)), and the average iteration number is about 15.

B. Choice of the Prediction Horizon

Comparative experiments were carried out for different prediction horizons under the driving cycle of UDDS. The simulation results are presented in Table I. It can be concluded that, as the prediction horizon increases, fuel benefits increase but converge to a limit, and the average iteration number of the proposed solver increases steadily. Therefore, the choice of the prediction horizon is a tradeoff between a preferable fuel-saving performance and an acceptable computational burden. Within the computational capacity of the ADAS hardware, prediction horizon should be chosen as long as possible, at least longer than 4 s.

C. Effect of the Average Speed

The effect of the average speed on fuel-saving performance is studied for the proposed PCC system. Given that the average speed of the host vehicle is determined by the speed of the preceding vehicle, the preceding vehicle is controlled by a driver model to track different speed profiles. The different speed profiles are obtained by scaling a specified speed profile (Fig. 7(a)),

TABLE I
COMPARISON FOR DIFFERENT PREDICTION HORIZONS

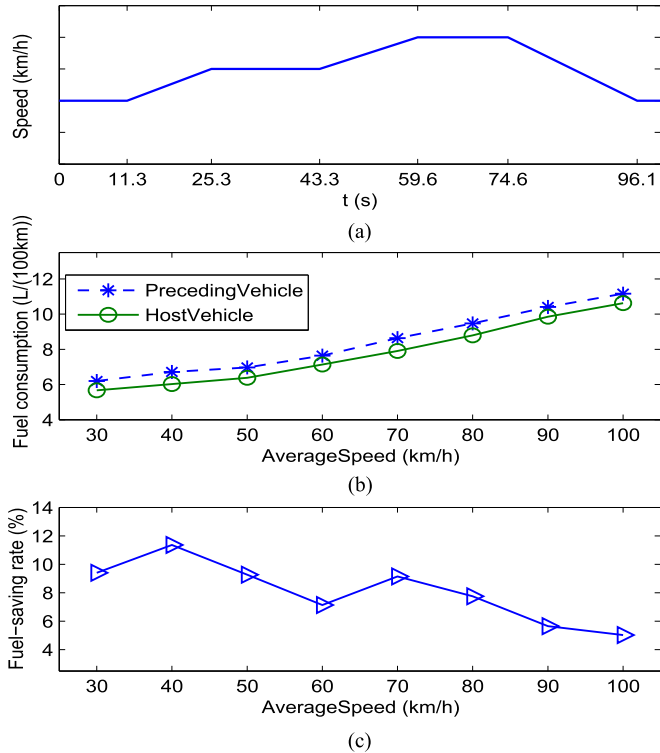| Prediction horizon (s)	0.5	1	2	3	4	5	6	7	8	9	10	20
Fuel benefits (%)	4.0	6.1	7.3	8.2	11.0	11.0	10.8	10.9	10.8	10.9	10.8	11.6
Average iteration number	11.2	12.0	13.0	13.8	14.4	14.8	15.0	15.1	15.3	15.4	15.5	15.8

Fig. 7. Performance under different average speeds. (a) A specified speed profile. (b) Fuel consumption. (c) Fuel-saving rate.

Fig. 8. Experimental platform.

TABLE II
CONTROLLER PARAMETERS

Symbol	Description	Value[un.]
κ, κ_1	weighting coefficients	0.9, 0.7
κ_2, κ_3	weighting coefficients	0.5, 1
σ, σ_v	conservative coefficient	0.8, 0.6
ε	tolerance	0.05
β_1, β_2	sharpness coefficients	0.5, 0.5
γ_1, γ_2	range coefficients	40, 5
$s_{min,0}$	minimum inter-vehicle distance	$0.2m$
τ_{min}	minimum time headway	$0.55s$

which consists of acceleration, constant speed, and deceleration conditions. The host vehicle is controlled by the proposed PCC to follow the preceding vehicle with a fixed gear ratio. Corresponding results are shown in Fig. 7. As shown in Fig. 7(b), the fuel consumptions of the preceding vehicle and the host vehicle increase with the increase of the average speed. However, it can be concluded from Fig. 7(c) that, as the average speed increases, the fuel-saving rate decreases approximately.

VI. EXPERIMENTAL RESULTS

The experimental platform is a production SUV, which is shown in Fig. 8. The PCC system consists of fuel consumption meter, GPS, INS, mobileye camera, rapid prototyping-system MicroAutoBoxII (with 900 MHz clock frequency, PPC750 GL Power PC processor), human-machine interface, and vehicle gateway. The Mobileye camera is used to measure the speed of the preceding vehicle and the inter-vehicle distance, and the mobileye system also provides a recommended target vehicle. The vehicle gateway is used to manage vehicle-to-camera communication. In real vehicle implementation, the system sampling interval is 0.01 s. The important controller parameters are given in Table II. Through large amount of experiments, the prediction

horizon is chosen as 7 s, and the discretization time interval in the prediction horizon is set as 0.1 s.

A. Control Performance Analysis

To show the control performance of the proposed control scheme, experiments are carried out in open traffic environment. The use of HD map is first represented. After that, from the perspective of engine operating point, the reason why the proposed PCC can save fuel is discussed.

1) HD map: The HD map provides near-term future information, which consists of speed limit, slope, curvature and positioning message. When the road is straight, the curvature radius in Eq. (30) is set as 15000 m or −15000 m. The sign of the curvature radius indicates left turn or right turn. Similarly, the sign of the slope indicates uphill or downhill. The curvature radius of the road is translated into the speed limit on the basis of vehicle location information. The corresponding experimental results are shown in Fig. 9. As a result of the offset of speed limit and curvature information, the vehicle is forced to slow down in advance. Although the speed of the preceding vehicle is above speed limit, the host vehicle speed will not exceed this limit.

2) Engine Operating Point: To show the mechanism of fuel saving, the performances of a traditional ACC and the proposed
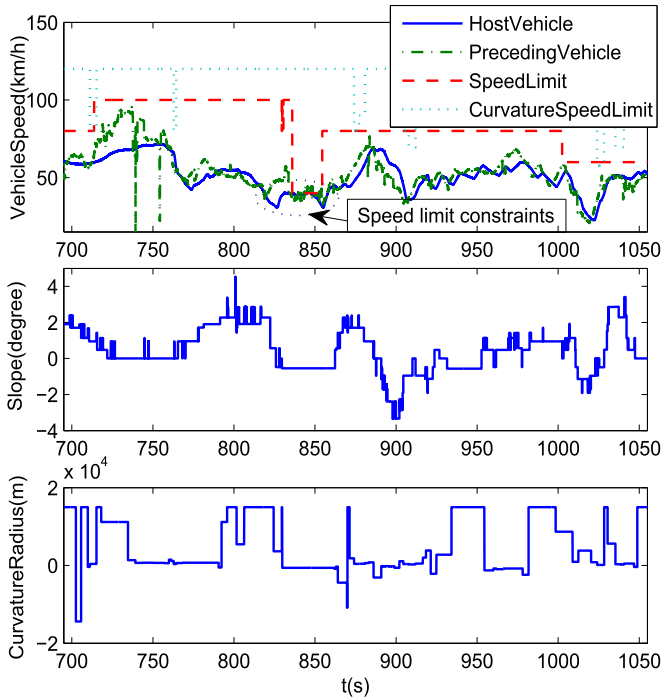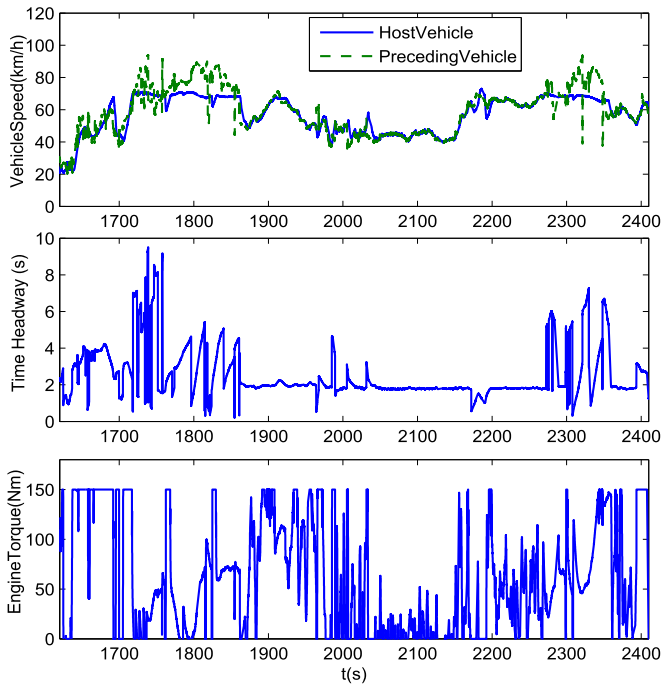
Fig. 9.   Control performance of PCC with HD map.

Fig. 10.   Control performance of traditional ACC.

Fig. 11.   Control performance of the proposed PCC.

(a) ACC

(b) PCC

Fig. 12.   Engine operating points.

PCC are experimentally compared, and the results are shown in Fig. 10 and Fig. 11. The traditional ACC performs the function of car-following by maintaining a constant time headway. However, the proposed PCC does not need the accurate control of time headway. As shown in Fig. 10 and Fig. 11, compared with the traditional ACC, the proposed PCC provides an optimal engine torque to minimize fuel consumption. Notably, the dither of the engine torque of PCC is considerably less than that of the traditional ACC. This behavior definitely helps save fuel. The
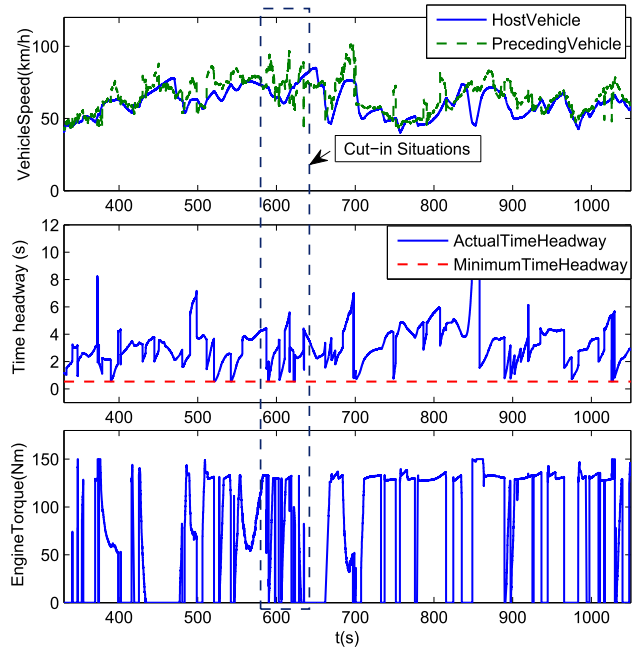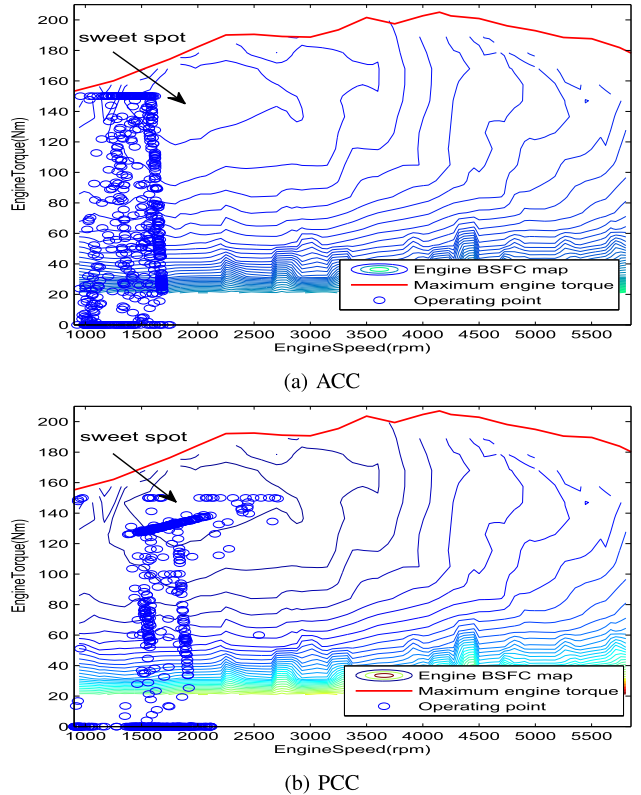
dashed box inset in Fig. 11 shows that the proposed PCC has good compatibility with cut-in situations. In addition, as can be seen from Fig. 11, the actual time headway does not exceed the minimum time headway. The constraints of (18c) and (18g) can be satisfied by the schedule solution.

Finally, the engine operating points of Fig. 10 and Fig. 11 are given in Fig. 12, where the BSFC map is given to better illustrate

TABLE III
COMPARISON RESULTS WITH A CRUISE SPEED SET OF $70km/h$

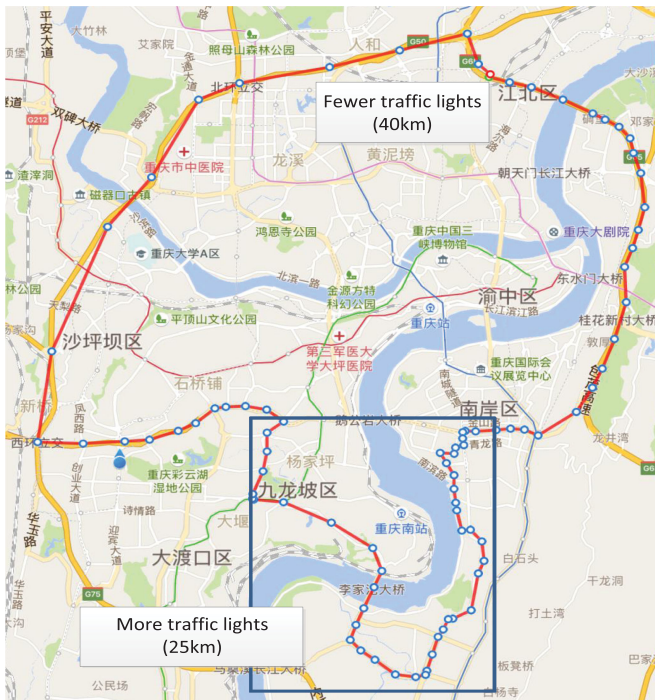| test	system	test time	average speed (km/h)	mileage (km)	fuel consumption ($L/100km$)
1	ACC	11:50-12:36;11:55-12:36	51.7	75	7.992
	PCC	12:51-13:32;10:40-11:26	52.7	75	7.492
2	ACC	16:49-17:39	46.4	39	8.820
	PCC	15:37-16:31	42.8	39	7.850
3	ACC	14:35-15:24	46.5	38	8.120
	PCC	15:34-16:43	43.2	36	7.545
4	ACC	11:53-12:29	60	37	8.208
	PCC	10:54-11:35	54.6	37	7.580

Fig. 13.   Experimental route.

Fig. 14.   Comparison of fuel consumption.

the mechanism of fuel saving and to compare the fuel efficiency of the operating points. The total number of observations is 75000, and the span of time is 750 s. The figure shows that the number of operating points in high efficiency area (sweet spot with a lower fuel consumption rate) is greater than that of the traditional ACC.

B. Comparison of Fuel Consumption

To further evaluate the fuel economy of the proposed PCC system, comparative experiments are conducted in an open traffic environment. The selected test path is a urban road, which is shown in Fig. 13. It consists of road sections with fewer traffic lights (40 km) and road sections with more traffic lights (25 km). There are many longitudinal slopes on the test path. The near-term future information of HD map is used in PCC, but not in ACC. To obtain the same traffic flow, the test times are ensured to be as consistent as possible in the comparative experiments. In case of emergency and long-term low-speed conditions, the system of PCC will deactivate, and the driver will take over. The results of the comparison are given in Table III. The total
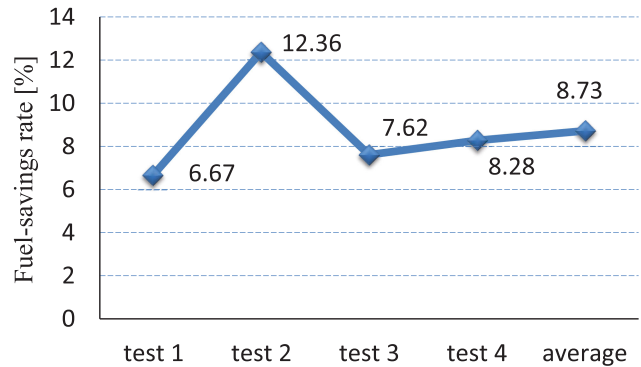
test mileage is 376 km. In fact, PCC mainly operated in car-following mode under the test conditions, wherein the traffic flow volume was relatively large. As can be seen from tests 2, 3 and 4, although the average speed of the vehicle with ACC is greater than that of the vehicle with PCC, the fuel consumption of the latter is less than that of the former. The comparison of fuel consumption is given in Fig. 14. Compared with that of the vehicle with ACC, the average fuel-savings rate of the vehicle with PCC can reach 8.73%.

VII. CONCLUSION

A novel control scheme of PCC is proposed to minimize fuel consumption. The proposed PCC system uses HD map information, and the problem of the PCC is summarized as a nonlinear multiobjective optimization. The HD map provides near-term future information, which consists of speed limit, slope, curvature and positioning message. A novel shift-map is proposed to provide a schedule for different working conditions. Finally, the proposed control scheme is evaluated through the simulation and real vehicle implementation.

  i) Simulation results reveal that fuel consumption is noticeably reduced (up to 6%) under the speed profiles of UDDS and NEDC.
 ii) Experimental results show that the vehicle slows down in advance to satisfy the speed constraint in accordance with the future speed limit of HD map.
iii) BSFC map results show that the optimal engine torque of proposed PCC is likely to be in a high-efficiency region.
 iv) Comparative experiments performed over a 350 km route show that the average fuel-savings rate can reach 8.73%.

Future work will use more road and traffic information, such as traffic signals. On the basis of the obtainable future road conditions, the speed predictive model of the preceding vehicle will also be enhanced.

APPENDIX
CONVERGENCE ANALYSIS OF THE PROPOSED SOLVER

The bisection method is guaranteed to converge to a root of $\beth(\lambda^{(r)}(0))$ if $\beth(\lambda^{(r)}(0))$ is a continuous function defined on the interval $[\lambda_L, \lambda_U]$ and $\beth(\lambda_L)$ and $\beth(\lambda_U)$ have opposite signs.

Define the bounds of the possible costate variable as

$$\lambda_L \leq \inf_{\forall v \in \mathcal{D}, T_e \in \mathcal{U}} \lambda(0), \lambda_U \geq \sup_{\forall v \in \mathcal{D}, T_e \in \mathcal{U}} \lambda(0) \quad (31)$$

where $\mathcal{D}$ and $\mathcal{U}$ are the admissible sets. To determine the interval $[\lambda_L, \lambda_U]$, we assume that $\lambda_{\min}(k) \leq \lambda(k) \leq \lambda_{\max}(k)$ for $k \in [0, 1, \ldots, N-1]$ without loss of generality, where $\lambda_L = \lambda_{\min}(0)$ and $\lambda_U = \lambda_{\max}(0)$. By inserting $\varrho_5(k)$ into Eq. (24), the update equation becomes

$$\lambda(k) = \lambda(k+1) + B(k), \quad (32)$$

where $B(k) = 2\sum_{i=0}^{2} \iota_{i,2} T_e^i(k)(\frac{30 I_0 I_g(k)}{\pi r_w})^2 + \sum_{i=0}^{2} \iota_{i,1} T_e^i(k)$ $(\frac{30 I_0 I_g(k)}{\pi r_w}) - 2\kappa_1(v_{ref} - v(k))$. Obviously, we can find $B_{\max} > 0$ and $B_{\min} < 0$ that ensure $B(k) \in [B_{\min}, B_{\max}]$ for $\forall v \in \mathcal{D}, T_e \in \mathcal{U}$. Then,

$$\begin{aligned} \lambda_{\max}(k) &= \lambda_{\max}(k+1) + B_{\max}, \\ \lambda_{\min}(k) &= \lambda_{\min}(k+1) + B_{\min}, \end{aligned} \quad (33)$$

On the basis of the terminal condition (21b), define

$$\lambda_{\max}(N) = 2\kappa q > 0, \lambda_{\min}(N) = -2\kappa q < 0, \quad (34)$$

where $q = \sup_{\forall v \in \mathcal{D}} |v(N) - v_{ref}|$. Because $B_{\max} > 0$ and $B_{\min} < 0$, one can conclude $\lambda_{\max}(k) > 0$ and $\lambda_{\min}(k) < 0$ for $k \in [0, 1, \ldots, N-1]$. Using backward induction, the interval $[\lambda_{\min}(0), \lambda_{\max}(0)]$, i.e., $[\lambda_L, \lambda_U]$, can be determined from the interval $[\lambda_{\min}(N), \lambda_{\max}(N)]$.

By referring the update equation (32), the terminal condition is represented by

$$F(\lambda(0)) = \lambda(N) = \lambda(0) - \sum_{k=0}^{N-1} B(k). \quad (35)$$

Then, the integrated terminal function becomes

$$\beth(\lambda(0)) = \lambda(0) - \sum_{k=0}^{N-1} B(k) - 2\kappa(v(N) - v_{ref}). \quad (36)$$

Given that $B(k) \in [B_{\min}, B_{\max}]$ and $q = \sup_{\forall v \in \mathcal{D}} |v(N) - v_{ref}|$, the interval $[\lambda_L, \lambda_U]$ can be found such that $\beth(\lambda_L) < 0$ and $\beth(\lambda_U) > 0$. Then, because the function of (36) is continuous, there must be a root within the interval $[\lambda_L, \lambda_U]$.
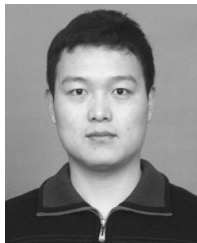
ACKNOWLEDGMENT

REFERENCES

[1] R. Sparrow and M. Howard, "When human beings are like drunk robots: Driverless vehicles, ethics, and the future of transport," *Transp. Res. Part C, Emerg. Technol.*, vol. 80, pp. 206–215, 2017.

[2] A. Morand, X. Moreau, P. Melchior, M. Moze, and F. Guillemard, "Crone cruise control system," *IEEE Trans. Veh. Technol.*, vol. 65, no. 1, pp. 15–28, Jan. 2016.

[3] S. E. Li, H. Peng, K. Li, and J. Wang, "Minimum fuel control strategy in automated car-following scenarios," *IEEE Trans. Veh. Technol.*, vol. 61, no. 3, pp. 998–1007, Mar. 2012.

[4] S. E. Li, X. Hu, K. Li, and C. Ahn, "Mechanism of vehicular periodic operation for optimal fuel economy in free-driving scenarios," *IET Intell. Transport Syst.*, vol. 9, no. 3, pp. 306–313, 2015.

[5] R. Schmied, H. Waschl, and L. Del Re, "Extension and experimental validation of fuel efficient predictive adaptive cruise control," in *Proc. Amer. Control Conf.*, 2015, pp. 4753–4758.

[6] L. Guo, B. Gao, Q. Liu, J. Tang, and H. Chen, "On-line optimal control of the gearshift command for multi-speed electric vehicles," *IEEE/ASME Trans. Mechatronics*, vol. 22, no. 4, pp. 1519–1530, Aug. 2017.

[7] A. Sciarretta, G. D. Nunzio, and L. L. Ojeda, "Optimal ecodriving control: Energy-efficient driving of road vehicles as an optimal control problem," *IEEE Control Syst.*, vol. 35, no. 5, pp. 71–90, Oct. 2015.

[8] T. Stanger and L. D. Re, "A model predictive cooperative adaptive cruise control approach," in *Proc. Amer. Control Conf.*, 2013, pp. 1374–1379.

[9] S. Li, K. Li, R. Rajamani, and J. Wang, "Model predictive multi-objective vehicular adaptive cruise control," *IEEE Trans. Control Syst. Technol.*, vol. 19, no. 3, pp. 556–566, May 2011.

[10] V. L. Bageshwar, W. L. Garrard, and R. Rajamani, "Model predictive control of transitional maneuvers for adaptive cruise control vehicles," *IEEE Trans. Veh. Technol.*, vol. 53, no. 5, pp. 1573–1585, Sep. 2004.

[11] F. Bu, H. S. Tan, and J. Huang, "Design and field testing of a cooperative adaptive cruise control system," in *Proc. Amer. Control Conf.*, 2010, pp. 4616–4621.

[12] M. Barth and K. Boriboonsomsin, "Energy and emissions impacts of a freeway-based dynamic eco-driving system," *Transp. Res. Part D Transport Environ.*, vol. 14, no. 6, pp. 400–410, 2009.

[13] P. Kachroo, N. Shlayan, S. Roy, and M. Zhang, "High-performance vehicle streams: Communication and control architecture," *IEEE Trans. Veh. Technol.*, vol. 63, no. 8, pp. 3560–3568, Oct. 2014.

[14] M. A. S. Kamal, M. Mukai, J. Murata, and T. Kawabe, "Ecological vehicle control on roads with up-down slopes," *IEEE Trans. Intell. Transp. Syst.*, vol. 12, no. 3, pp. 783–794, Sep. 2011.

[15] E. Hellström, M. Ivarsson, J. Åslund, and L. Nielsen, "Look-ahead control for heavy trucks to minimize trip time and fuel consumption," *Control Eng. Pract.*, vol. 17, no. 2, pp. 245–254, 2009.

[16] S. Park, H. Rakha, K. Ahn, and K. Moran, "Predictive eco-cruise control: Algorithm and potential benefits," in *Proc. Integr. Sustain. Transp. Syst.*, 2011, pp. 394–399.

[17] M. Miyatake, M. Kuriyama, and Y. Takeda, "Theoretical study on eco-driving technique for an electric vehicle considering traffic signals," in *Proc. IEEE 9th Int. Conf. Power Electron. Drive Syst.*, 2011, pp. 733–738.

[18] L. Guo, B. Gao, Y. Gao, and H. Chen, "Optimal energy management for HEVs in eco-driving applications using bi-level MPC," *IEEE Trans. Intell. Transp. Syst.*, vol. 18, no. 8, pp. 2153–2162, Aug. 2017.

[19] B. Asadi and A. Vahidi, "Predictive cruise control: Utilizing upcoming traffic signal information for improving fuel economy and reducing trip time," *IEEE Trans. Control Syst. Technol.*, vol. 19, no. 3, pp. 707–714, May 2011.

[20] M. A. S. Kamal, M. Mukai, J. Murata, and T. Kawabe, "Model predictive control of vehicles on urban roads for improved fuel economy," *IEEE Trans. Control Syst. Technol.*, vol. 21, no. 3, pp. 831–841, May 2013.

[21] J. Ploeg, B. T. M. Scheepers, E. V. Nunen, and N. V. D. Wouw, "Design and experimental evaluation of cooperative adaptive cruise control," in *Proc. Int. IEEE Conf. Intell. Transp. Syst.*, 2011, pp. 260–265.

[22] E. Hellström, J. Åslund, and L. Nielsen, "Design of an efficient algorithm for fuel-optimal look-ahead control," *Control Eng. Pract.*, vol. 18, no. 11, pp. 1318–1327, 2010.

[23] L-H Luo, H. Liu, P. Li, and H. Wang, "Model predictive control for adaptive cruise control with multi-objectives: comfort,fuel-economy, safety and car-following," *J. Zhejiang Univ.-Science A(Appl. Phys. Eng.)*, vol. 11, no. 3, pp. 191–201, 2010.

[24] J. Marzbanrad and N. Karimian, "Space control law design in adaptive cruise control vehicles using model predictive control," *Proc. Institution Mech. Eng. Part D J. Automobile Eng.*, vol. 225, no. 7, pp. 870–884, 2011.

[25] S. Zhang, Y. Luo, K. Li, and V. Li, "Real-time energy-efficient control for fully electric vehicles based on explicit model predictive control method," *IEEE Trans. Veh. Technol.*, vol. 67, no. 6, pp. 4693–4701, Jun. 2018.

[26] H. Waschl, I. Kolmanovsky, M. Steinbuch, and L. D. Re, *Optimization and Optimal Control in Automotive Systems*. Berlin, Germany: Springer, 2014.

[27] N. Murgovski, L. M. Johannesson, and E. Bo, "Optimal battery dimensioning and control of a CVT PHEV powertrain," *IEEE Trans. Veh. Technol.*, vol. 63, no. 5, pp. 2151–2161, Jun. 2014.

[28] J. Wang and R. Rajamani, "Should adaptive cruise-control systems be designed to maintain a constant time gap between vehicles?" *IEEE Trans. Veh. Technol.*, vol. 53, no. 5, pp. 1480–1490, Sep. 2004.

[29] S. E. Li, Q. Guo, L. Xin, B. Cheng, and K. Li, "Fuel-saving servo-loop control for an adaptive cruise control system of road vehicles with step-gear transmission," *IEEE Trans. Veh. Technol.*, vol. 66, no. 3, pp. 2033–2043, Mar. 2017.

[30] P. A. Ioannou and C. C. Chien, "Autonomous intelligent cruise control," *IEEE Trans. Veh. Technol.*, vol. 42, no. 4, pp. 657–672, Nov. 1993.

[31] C. M. Martinez, M. Heucke, F. Y. Wang, B. Gao, and D. Cao, "Driving style recognition for intelligent vehicle control and advanced driver assistance: A survey," *IEEE Trans. Intell. Transp. Syst.*, vol. 19, no. 3, pp. 666–676, Mar. 2018.

[32] J.-J. Martinez and C. Canudas-de Wit, "A safe longitudinal control for adaptive cruise control and stop-and-go scenarios," *IEEE Trans. Control Syst. Technol.*, vol. 15, no. 2, pp. 246–258, Mar. 2007.

[33] Y. Yamamura, M. Tabe, M. Kanehira, and T. Murakami, "Development of an adaptive cruise control system with stop-and-go capability," SAE Technical Paper, Tech. Rep. 2001-01-0798, Detroit, Michigan, USA, 2001.

[34] E. D. Dickmanns and A. Zapp, "Autonomous high speed road vehicle guidance by computer vision1," *IFAC Proc. Vol.*, vol. 20, no. 5, pp. 221–226, 1987.

[35] S.-H. Ha and H.-T. Jeon, "Development of intelligent gear-shifting map based on radial basis function neural networks," *Int. J. Fuzzy Logic Intell. Syst.*, vol. 13, no. 2, pp. 116–123, 2013.

[36] M. Nagaoka and K. Oda, "Gear shift control for an automatic transmission of a vehicle," US Patent 4,584,906, April 29 1986.

Bingzhao Gao received the B.S. and M.S. degrees in vehicle engineering from Jilin University, Changchun, China, in 1998 and 2002, respectively, and the Ph.D. degrees in mechanical engineering from Yokohama National University, Yokohama, Japan, and in control engineering from Jilin University, in 2009. He is currently a Professor with Jilin University. His current research interests include vehicle powertrain control and vehicle stability control.

Hong Chen (M'02–SM'12) received the B.S. and M.S. degrees in process control from Zhejiang University, Zhejiang, China, in 1983 and 1986, respectively, and the Ph.D. degree in system dynamics and control engineering from the University of Stuttgart, Stuttgart, Germany, in 1997. Since 1999, she has been a Professor with Jilin University, Changchun, China, where she is currently as a Tang Aoqing Professor and as the Director of the State Key Laboratory of Automotive Simulation and Control. Her current research interests include model predictive control, optimal and robust control, and nonlinear control and applications in mechatronic systems focusing on automotive systems.

Ning Bian received the M.S. degree in electrical and information technology from the Technical University of Munich, Munich, Germany, and the Ph.D. degree in automotive control and intelligent safety from the University of Duisburg-Essen, Duisburg, Germany. He has worked more than 7 years for integrated chassis control and ADAS in research and development center of BMW Group and in System and Technology Center of Continental AG Germany. He is currently the Acting Director of Intelligent Connected Vehicle Division with DongFeng Motor Group Technical Center with interests in ADAS, Automated Driving, Chassis Control.

Hongqing Chu received the B.S. degree in vehicle engineering from the Shandong University of Technology, Zibo, China, in 2012, and the Ph.D. degree in control theory and control engineering from Jilin University, Changchun, China, in 2017. He is currently a Postdoctoral Fellow with the Department of Vehicle Engineering, Jilin University, Changchun, China. His current research interests include advanced driver-assistance systems, nonlinear control of DC motor drive, and vehicle powertrain control.

Lulu Guo received the B.S. degree in vehicle engineering from Jilin University, Changchun, China, in 2014, where he is currently working toward the Ph.D. degree in control theory and engineering. His current research interests include advanced vehicle powertrain control, energy management of hybrid electric vehicles, and optimal control theory and its applications.

Jianguang Zhou received the Ph.D. degree in mechanical engineering from the University of Hiroshima, Higashihiroshima, Japan, with major in combustion science of internal combustion engines. He has worked for more than 10 years in the Technical Center of Isuzu Motors Ltd., and Nissan Motors Ltd., for developing passenger car diesel engines and gasoline engines. In 2008, he joined Dongfeng Motor Corporation, Technical Center. He is currently the Vice-Director, who takes charge of Dongfeng self-brand vehicles development in the field of engines, new energy vehicles, ECU and intelligent connected vehicles.